PLOS ONE

RESEARCH ARTICLE

Linear interactions between intraocular, intracranial pressure, and retinal vascular pulse amplitude in the fourier domain

Anmar Abdul-Rahman[1,2]*, **William Morgan**[2,3], **Ying Jo Khoo**[3,4], **Christopher Lind**[5,6], **Allan Kermode**[7,8], **William Carroll**[7], **Dao-Yi Yu**[2,3]

1 Department of Ophthalmology, Counties Manukau District Health Board, Auckland, New Zealand, **2** Centre for Ophthalmology and Visual Science, The University of Western Australia, Perth, Australia, **3** Lions Eye Institute, University of Western Australia, Perth, Australia, **4** Royal Perth Hospital, Perth, Australia, **5** Neurosurgical Service of Western Australia, Sir Charles Gairdner Hospital, Nedlands, Western Australia, Australia, **6** Department of Surgery, University of Western Australia, Crawley, Western Australia, Australia, **7** Centre for Neuromuscular and Neurological Disorders, Perron Institute for Neurological and Translational Science, Sir Charles Gairdner Hospital Department of Neurology and Clinical Neurophysiology, Nedlands, Western Australia, Australia, **8** Institute for Immunology and Infectious Disease, Murdoch University Faculty of Health Sciences, Murdoch, Western Australia, Australia

* anmar_rahman@hotmail.com

Abstract

Purpose

To compare the retinal vascular pulsatile characteristics in subjects with normal (ICP_n) and high (ICP_h) intracranial pressure and quantify the interactions between intraocular pressure, intracranial pressure, and retinal vascular pulse amplitude in the Fourier domain.

Materials and methods

Twenty-one subjects were examined using modified photoplethysmography with simultaneous ophthalmodynamometry. A harmonic regression model was fitted to each pixel in the time-series, and used to quantify the retinal vascular pulse wave parameters including the harmonic regression wave amplitude (HRW_a). The pulse wave attenuation was measured under different ranges of induced intraocular pressure (IOP_i), as a function of distance along the vessel (V_{Dist}). Intracranial pressure (ICP) was measured using lumbar puncture. A linear mixed-effects model was used to estimate the correlations between the Yeo-Johnson transformed harmonic regression wave amplitude (HRW_{a-YJt}) with the predictors (IOP_i, V_{Dist} and ICP). A comparison of the model coefficients was done by calculating the weighted Beta (β_x) coefficients.

Results

The median HRW_a in the ICP_n group was higher in the retinal veins (4.563, interquartile range (IQR) = 3.656) compared to the retinal arteries (3.475, IQR = 2.458), p<0.0001. In contrast, the ICP_h group demonstrated a reduction in the median venous HRW_a (3.655, IQR = 3.223) and an elevation in the median arterial HRW_a (3.616, IQR = 2.715), p<0.0001.

Interactions of the pulsation amplitude with ICP showed a significant disordinal interaction and the loss of a main effect of the Fourier sine coefficient (b_{n1}) in the ICP_h group, suggesting that this coefficient reflects the retinal vascular response to ICP wave. The linear mixed-effects model (LME) showed the decay in the venous (HRW_{a-YJt}) was almost twice that in the retinal arteries (−0.067±0.002 compared to −0.028±0.0021 respectively, p<0.00001). The overall interaction models had a total explanatory power of (conditional R^2) 38.7%, and 42% of which the fixed effects explained 8.8%, and 5.8% of the variance (marginal R^2) for the venous and arterial models respectively. A comparison of the damping effect of V_{Dist} and ICP showed that ICP had less influence on pulse decay than distance in the retinal arteries (β_{ICP} = -0.21, se = ±0.017 compared to $\beta_{V_{Dist}} = -0.26$, se = ±0.019), whereas the mean value was equal for the retinal veins (venous $\beta_{V_{Dist}} = -0.42$, se = ±0.015, β_{ICP} = -0.42, se = ±0.019).

Conclusion

The retinal vascular pulsation characteristics in the ICP_h group showed high retinal arterial and low venous pulsation amplitudes. Interactions between retinal vascular pulsation amplitude and ICP suggest that the Fourier sine coefficient b_{n1} reflects the retinal vascular response to the ICP wave. Although a matrix of regression lines showed high linear characteristics, the low model explanatory power precludes its use as a predictor of ICP. These results may guide future predictive modelling in non-invasive estimation of ICP using modified photoplethysmography.

Introduction

Changes in retinal hemodynamics are a consequence of a complex interaction between intraocular pressure (IOP), intracranial pressure (ICP), and systemic blood pressure [1, 2]. The balance of cerebrospinal fluid, blood supply, and cerebral parenchymal volume is required for ICP homeostasis [3]. Although the outflow of cerebrospinal fluid into the venous circulation accommodates a moderate increase in ICP, once the buffering mechanisms are decompensated, ICP rises to the level of intravascular pressure in the cerebral arterioles [4], consequently changes occur in the retinal vasculature. Increased retinal venous pressure causes venous distension, which subsequently reduces venous compliance [5–7]. Several human and animal studies confirmed the strong linear relationship between retinal venous hemodynamic parameters and ICP. Using ophthalmodynamometry to assess the correlation between venous opening pressure and ICP, Firsching et al. found a linear correlation (R) of 0.983 (p<0.001), Motshcmann et al. similarly reported a correlation of 0.968 [8]. Querfurth et al. measured the correlation of venous opening pressure (R = 0.87) in addition to the inverse correlation of the arterial pulsatility indices for both the ophthalmic and central retinal arteries (R = 0.66) they described an empiric index by combining both venous and arterial parameters (venous opening pressure/Gosling Pulsatility Index [GPI]) that was more strongly correlated with absolute ICP than either parameter alone (R = 0.95, p <0.005) [9]. Similarly, Hayreh et al., in a primate study, reported ophthalmic venous pressure to be linearly correlated with ICP (R^2 0.8–1, p = 0.01) when measured using direct cannulation [5]. The influence of ICP on the retinal arterial system is more controversial. In 1927 Baurman provided the earliest description of retinal

hemodynamic changes with acute elevation of the ICP; using ophthalmodynamometry he reported a linear relationship between ICP and retinal venous pressure [10]. Using the same methodology Berens and co-workers found a raised pressure in the central retinal artery independent of systemic blood pressure [11]. In contrast in a primate model, Hayreh et al. demonstrated a high positive correlation between the systemic blood pressure and ophthalmic artery pressure, they reported systolic ophthalmic artery pressure was 71% of the systolic blood pressure and the diastolic ophthalmic artery pressure 87% of the diastolic systemic pressure, the correlation between the diastolic ophthalmic and systemic blood pressures was maintained on raising ICP to 35mmHg. At higher ICPs, and the systolic ophthalmic artery pressure dropped to 47% of the systolic blood pressure. It was thought that this was due to a "cuffing effect" of the raised ICP on the intracranial portion of the ophthalmic artery, which did not interfere with the diastolic ophthalmic artery pressure [5]. It is likely that a complex interaction between IOP, local anatomical factors, retinal hemodynamics, ICP, retrolaminar tissue pressure, and systemic blood pressure influence this predictive accuracy [12]. This complex interaction of factors is traditionally summarised by the translaminar pressure gradient and difference. In these assumptions, cerebrospinal fluid pressure is considered as an opposing force to intraocular pressure at the lamina cribrosa [13–16]. Here, venous pulsations are thought to cease when ICP exceeds central venous pressure. Based on this assumption, several investigators have attempted to define this critical ICP threshold value, Walsh et al. [17]. showed that the mean cerebrospinal fluid pressure for obliterating pulsations was 200±25 mm Water. Similarly, Kahn and Cherry [18], Levin [19] and Rosenberg [20] showed ICP must be less than 190–195 mm Water when pulsations are present [21]. Yet paradoxically these reduced models and simplified assumptions have not yielded an adequate predictive power when ICP prediction is concerned [3, 22, 23]. The paradox may be due to unaccounted-for non-linear dynamics or inter and intra-individual variability of the predictors, which may further limit the practical applicability of these reduced models.

Uncertainty principles refer to a meta-theorem in Fourier analysis. They are expressed as inequality equations and convey the general concept that a non-zero function and its Fourier decomposition cannot be localized to arbitrary precision [24]. Of the uncertainty principles, the Heisenberg-Gabor uncertainty principle defines the limit of the resolution of a signal in both time and frequency. Described in 1946 in Gabor's work on the theory of communication, it states that information cannot be localized simultaneously in both time and frequency [25]. Hence, the principle asserts that there exists a tradeoff between temporal (Δt) and spectral (Δf) resolution [26]. This is encapsulated by the mathematical identity:

$$\Delta f \cdot \Delta t \geq C$$

Where (C) is a constant with a value dependent on the methodology employed in frequency measurement. Here, for the inequality to remain true the reduction in temporal resolution demands an increase in frequency resolution. Additional to the aforementioned unique resolution property and hence information content, frequency domain analysis has the advantage of de-noising the decomposed signal, a characteristic that is favorable in artifact-prone ophthalmic imaging. Consequently, hemodynamic parameters can exist as a distinct property of the frequency domain, such as input impedance (defined as the ratio of the pressure to flow harmonics [27]), dispersion (defined as wave velocity dependence on harmonic frequency [28]), and harmonic amplitude attenuation (defined as the decay in harmonic amplitude as a function of distance [29]). Modified Photoplethysmography is a novel non-invasive technique of measurement of the retinal vascular pulse amplitude and timing characteristics in the Fourier domain. A plethysmography wave has non-periodic and periodic components [30]. Therefore,

the harmonic regression model used to analyze the retinal vascular pulse wave consists of a linear spline to model the non-periodic component and an autoregressive error component used to represent the trend in the time series. The periodic component is represented by a Fourier series composed of the first two harmonics [31]. Akaike Information Criterion is used to determine the maximum extractable frequencies from the images. Generally, the number of extractable harmonics is dependent on the signal-to-noise ratio. Theoretical studies on vascular pressure-flow waveforms indicate that there are a larger number of extractable harmonics, Krovetz et al. [32]. analyzed the harmonics of intracardiac and arterial pressure waves, and they reported that 3–10 harmonics were required to reproduce the pressure waveforms, however, differential pressures and derivatives, appeared to contain six-fold the number of higher-frequency harmonics [32]. From other studies, the first two harmonics account for approximately 85% of the pulsatile portions of pressure and flow in large arteries, which may indicate that lower-order harmonics are sufficient to represent these waveforms [33]. Practically, there is a fundamental limit to the number of harmonics that can be extracted. Beyond the tenth harmonic component, the harmonic magnitudes of the aortic pressure pulse and aortic flow pulse are negligible. This limit arises from sampling factors and signal noise, as to accurately reconstruct the original waveform, the Nyquist criterion requires a sampling frequency of at least twice the highest-frequency content. As a result, frequency-domain methods rely on identifying a suitable frequency band or harmonic range that is less susceptible to noise [27, 34–36]. Although general principles around the Nyquist limit apply to harmonic pulse wave analysis, comparisons of the extractable harmonics in these studies with our work are not possible due to differences in the measurement parameter, methodology, and the vessel characteristics.

In this study, we quantified the correlation between the linear terms of pulse amplitude in the frequency domain for both the retinal venous and the arterial systems at different distances along the vessels and under a range of induced IOP values; generated by ophthalmodynamometry in patients with normal and high ICP. In order to ascertain the variance captured by a linear mixed effects model and further our understanding of the limit of linear models in the prediction of ICP non-invasively. Hence, the parameters of linear models with and without interactions between the predictors are estimated. Here, we make no assumptions regarding the physiology and physics of collapsible vessel behavior at pressure discontinuities.

Materials and methods

Study recruitment

Participants were referred to the Lions Eye Institute over five years (2015–2020) from the Neurology and Neurosurgery Departments and were to undergo lumbar puncture for suspicion of idiopathic intracranial hypertension. Gender is a well recognised risk factor in this disorder with over 90% of patients affected with idiopathic intracranial hypertension are female [37]. This explains the gender bias in our study. Modified photoplethysmography, a form of ophthalmodynamometry, was performed on all subjects. This consists of a force transducer surrounding a central contact lens, which allows imaging of the optic disc under a dynamic range of induced intraocular pressures (IOP_i). Written consent was obtained from each of the participants. Study approval was obtained from the University of Western Australia Human Ethics Committee adhering to the tenets of the Declaration of Helsinki. Participants were required to have clear ocular media. Exclusion criteria included any previous history of retinal or optic nerve pathology and optical media opacity. There were a total of 21 patients in the study group, an ICP of 25 cm water was considered the upper normal limit [38]. Ten cases (20 eyes) were in the high intracranial pressure group (ICP_h>25cm water) and 8 cases (13 eyes) in the normal intracranial pressure group (ICP_n≤25cm water). Three cases (6 eyes) overlapped
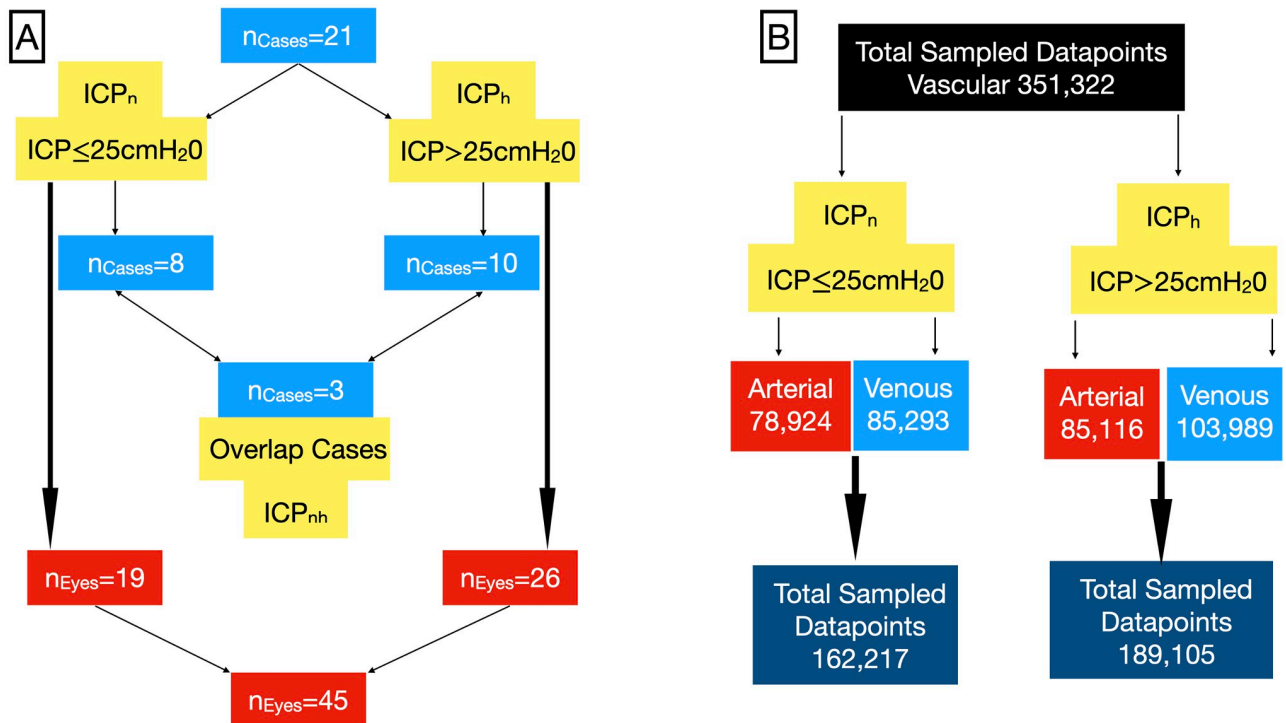
Fig 1. Classification of the study population and image data points. A) A total of 21 subjects were classified into two groups dependent on the intracranial pressure (ICP). An ICP of 25 cm water was the normal upper limit. B) A total of 351,322 data points were sampled from the images.

https://doi.org/10.1371/journal.pone.0270557.g001

between the two groups as a result of interchanging between the ICP_n to the ICP_h groups. Therefore there were a total of 19 eyes in the ICP_n group and 26 eyes in the ICP_h group, giving a total of 45 eyes in the study as three eyes were excluded from the analysis due to poor image quality (Fig 1). A total of 351,322 data points were sampled from the images of the study group: 162,217 arterial and 189,105 venous data points (Fig 1).

Image acquisition

All participants underwent visual acuity and slit-lamp examination. Baseline intraocular pressure was measured with Goldmann contact tonometry. Photoplethysmography was performed using the Meditron ophthalmodynamometer (Meditron GmbH, Poststrasse, Völklingen, Germany). This device consists of a sensor ring, which measures the force surrounding a central Goldmann three-mirror contact lens. The optic nerve head was continuously imaged biomicroscopically during the examination through the ophthalmodynamometer central contact lens. The examination was repeated approximately 10 times for each subject to attain a range of ophthalmodynamometry values for each eye, allowing a video segment to span at least five consecutive cardiac cycles. Examination duration varied depending on the number and length of the video recordings. A maximum of 2–3 minutes of light exposure per eye was estimated for the duration of the test. Slit-lamp light intensity was set at the minimum setting allowed for imaging to improve subject comfort and compliance with the test. Although the effects of ocular warming on the retinal vascular pulse wave is a theoretical possibility, in our study the effect is likely to be negligible due to the brief duration of exposure and the lower light intensities

compared to those reported in studies of the effect of temperature on retinal blood flow [39, 40].

Videos showing excessive motion artifact, reflection from the optical media, or decentration of the optic nerve in the image sequence for less than three consecutive cardiac cycles were rejected from the analysis. The ophthalmodynamometric force (ODF) displayed as Meditron units (mu) was converted to induced intraocular pressure (IOP_i) estimated from the baseline intraocular pressure (IOP_b) using the formula described in previous work [41]:

$$IOP_i = 0.89 \cdot ODF + IOP_b$$

An imaging slit-lamp (Carl Zeiss, Germany) with a digital camera (Canon 5D Mark III, Japan) was used to record multiple video sequences of at least three cardiac cycles in length, each at a rate of 25 frames/second. A pulse oximeter (Nellcor N65, Covidien, Mansfield, MA) was applied to the right index finger; the audio signal from the pulse oximeter, captured with the video sequence of the optic nerve allowed synchronization of the retinal vascular pulse with the cardiac cycle as image analysis required timing of the retinal vascular pulse based on fractions of the cardiac cycle. A Single high-quality length video spanning three-cardiac cycles was extracted from each recording session.

Image analysis

Adobe Photoshop CS6 was in the image processing step, individual image frames were extracted from each video sequence and saved as Tagged Image File Format (TIFF) files. Each of these images was cropped to an array of pixels. All images from three cardiac cycles were analyzed in R statistical package using custom software [42]. Each data point was represented by the mean of the green channel intensity at time measured as a fraction of the cardiac cycle, rather than in seconds. The periodic trend component was modeled as a Fourier series expansion:

$$\mathscr{F}(f(t)_p) = a_0 + \sum_{n=1}^{\infty} a_n \cdot cos(n\pi t) + b_n \cdot sin(n\pi t)$$

$f(t)_p$ = The periodic component of the time series.
a_0 = Coefficient representing the mean of $f(t)_p$.
a_n = Coefficient of the cosine function of $f(t)_p$.
b_n = Coefficient of the sine function of $f(t)_p$.
n = Integer 0,1,2. . . etc representing the harmonic component.

Higher harmonic frequency model comparisons were conducted using Akaike Information Criterion. In most eyes the Akaike Information Criterion preferred models with first and second-order frequencies, therefore the final analysis was limited to the first and second harmonics (n1,2). Image analysis and segmentation are detailed in our previous work [29, 43].

Statistical analysis

A harmonic regression model was fitted to each pixel in the time-series, and used to quantify the retinal vascular pulse wave parameters including the harmonic regression wave amplitude (HRW_a). The model includes a Fourier series representation using the first and second harmonics, linear spline non-periodic component, and a first-order autoregressive error component. The model was applied to the retinal arteries and veins separately [29, 31, 44]. The distribution of the HRW_a and the majority of the Fourier coefficients were non-normal, therefore the median was used to measure central tendency, and dispersion was estimated using

Table 1. Estimated normality statistics.

	Non-Transformed	Yeo-Johnson Transformed	λ
Artery			
HRW_a	35.4325	6.5197	-0.0635
a_{n1}	2.6041	1.9499	0.9406
b_{n1}	12.5317	12.7153	0.9747
a_{n2}	5.6896	5.7172	0.8976
b_{n2}	5.9913	5.8878	1.0475
Vein			
HRW_a	63.0409	7.5351	-0.1684
a_{n1}	21.6354	5.9935	0.7561
b_{n1}	23.2509	23.0105	1.0128
a_{n2}	11.1054	9.856	1.0871
b_{n2}	12.5743	12.338	1.0561

Estimated normality statistics (Pearson P/df) comparing non-transformed with Yeo-Johnson Power transformed parameters of the Fourier series. The lower the normality statistic the more favourable approximation to a normal distribution. Lambda (λ) is the critical parameter for the Yeo-Johnson transformation.

interquartile range (IQR), and the range was also computed. Hypothesis tests were conducted for both the non-normalized and normalized data using the Wilcoxon test with Bonferroni correction, and multivariate analysis of variance (MANOVA) respectively. Multifactoral Homogeneity of variance was tested using the Levene test.

Yeo-Johnson transformation (YJ_t) was used to normalise the harmonic regression waveform amplitude (HRW_a), the cosine ($a_{n1,2}$) and the sine ($b_{n1,2}$) coefficients of the first and second Fourier harmonics. The justification of this approach was evaluated by the transformation-estimating functions in the bestNormalize package in R [45], which uses the estimated normality statistics (Pearson P / df) statistic in recommending a transformation method and the required parameters (Table 1). The lower the normality statistic, the more favorable is the approximation to a normal distribution. This transformation is a suitable approach for negative values [46, 47]. These transformations are defined by:

$$\psi(\lambda, y) = \begin{cases} \dfrac{(y+1)^{\lambda}}{\lambda} & if \quad \lambda \neq 0, \ y \geq 0 \\ log(y+1) & if \quad \lambda = 0, \ y \geq 0 \\ \dfrac{(-[y+1])^{2-\lambda} - 1}{2 - \lambda} & if \quad \lambda \neq 2, \ y < 0 \\ -log(-y+1) & if \quad \lambda = 2, \ y < 0 \end{cases}$$

If the data point is strictly positive, then the YJ_t is the same as the Box-Cox power transformation of (y+1). If strictly negative, then the YJ_t is the Box-Cox power transformation of (-y+1), but with power 2-λ. With both negative and positive values, the transformation is a mixture of these two methods [46]. The Estimated Normality Statistics (Pearson P / degrees of freedom) were used, this showed favorable transformation criteria for YJ_t data when compared against both non-transformed and Logarithmic transformation with translation (Table 1).

Interaction plots were created to determine the Fourier coefficients influenced by increased ICP. The regression equations consisted of a five-level hierarchical linear mixed-effects model, with and without interaction effects was used to analyze the correlations of both the HRW_a and individual trigonometric harmonic coefficients [cosine ($a_{n1,2}$), sine ($b_{n1,2}$)] of the first and second harmonics with the predictors, ICP, the distance along the vessel (V_{dist}) and induced intraocular pressure (IOP_i). Linear mixed effect model goodness fit statistics were assessed using conditional R^2, which describes the proportion of variance explained by all factors in the model including the predictors, ICP, V_{dist} and IOP_i and random factors (subject, age, gender, laterality "right/left", hemiretinal location "superior/inferior"), whereas marginal R^2 describes the proportion of variance explained by the predictors ICP, V_{dist}, and IOP_i alone [48]. Beta coefficients were computed to compare effect size in the multivariate regression models.

Results

Study population

The age of the population demonstrated a bimodal distribution with a mean of 30 years (range 17–47 years). There were 20 (95.2%) females and 1 (4.8%) male. Whereas in the ICP_n group the median was 18.50 cm water (range 9.50–24, IQR = 5.5), the corresponding values in the ICP_h group were 31cm water (range 25.50–68, IQR = 11).

Harmonic regression waveform amplitude and Fourier coefficients

The median venous HRW_a was higher in the ICP_n group (4.563, range = 0.228–14.434, IQR = 3.656) compared to the ICP_h group (3.655, range = 0.339–11.983, IQR = 3.223), this was in contrast to the arterial pulsation amplitude where the median arterial HRW_a was higher in the ICP_h group (3.616, IQR = 2.715, range = 0.338–9.983) compared to the ICP_n group (3.475, IQR = 2.458, range = 0.353–9.233). Between (ICP_h and ICP_n) and within (artery and vein) group differences in the median pulsation amplitudes achieved statistical significance ($p < 0.0001$) for all, except the venous a_{n1} coefficient between groups and the $b_{n1,2}$ within in the ICP_h group (Table 2). Therefore there is a reduction in the venous and an increase in arterial pulsation in the ICP_h group (Fig 2). Yeo-Johnson transformation (YJ_t) was undertaken to normalize the HRW_a and the Fourier coefficients. As in the non-transformed Fourier terms, statistical significance in the differences between the mean HRW_a was sustained between the venous (1.502 and 1.368) and arterial (1.435 and 1.466)($p < 0.001$) of the ICP_n and ICP_h groups respectively. Between-group differences were statistically significant in all ($p < 0.001$) except the arterial a_{n2} coefficient. Both within and between-group heterogeneity of the variances was demonstrated using the Levene test ($p < 0.0001$) for the transformed and non-transformed Fourier terms.

Mixed effects linear regression model

Correlations between the predictors of the hierarchical multivariate linear regression were undertaken in the YJ_t transformation space. In a mixed-effects linear regression model correlating the amplitude of the terms of the Fourier equation with three predictors distance along the vessel (V_{Dist}) measured in millimeters (mm) from the center of the optic disc, intracranial pressure (ICP) measured in centimeters water (cm water) and induced intraocular pressure (IOP_i) measured in millimeters mercury (mmHg). There was a decay in the venous Yeo-Johnson transformed HRW_a with both predictors V_{Dist} and ICP. The slope of regression line correlating the HRW_a with V_{Dist} was -0.071±0.002 (p-value<0.00001) whereas that correlating with ICP was -0.0059±0.0004 (p-value<0.00001). There was amplification of the HRW_a as indicated

Table 2. Descriptive statistics.

Parameter	Site	Median	IQR	Min	Max	Range
ICP_n						
HRW_a	Artery	3.475	2.458	0.353	9.233	8.88
a_{n1}	Artery	0.078	1.469	-3.924	4.446	8.37
b_{n1}	Artery	-1.001	1.153	-4.61	4.088	8.699
a_{n2}	Artery	0.011	0.574	-2.505	2.755	5.26
b_{n2}	Artery	0.083	0.561	-3.388	3.258	6.647
HRW_a	Vein	4.563	3.656	0.228	14.434	14.207
a_{n1}	Vein	0.440[b]	2.057	-6.405	7.045	13.45
b_{n1}	Vein	-1.324	1.596	-7.211	5.573	12.785
a_{n2}	Vein	-0.072	0.685	-4.335	4.248	8.583
b_{n2}	Vein	0.130	0.623	-3.741	4.064	7.805
ICP_h						
HRW_a	Artery	3.616	2.715	0.338	9.983	9.645
a_{n1}	Artery	0.179	1.666	-4.826	4.749	9.576
b_{n1}	Artery	-1.029[w]	1.120	-4.937	4.37	9.307
a_{n2}	Artery	-0.015	0.605	-2.911	3.158	6.069
b_{n2}	Artery	0.063[w]	0.622	-3.022	3.256	6.277
HRW_a	Vein	3.655	3.223	0.339	11.983	11.645
a_{n1}	Vein	0.364[b]	1.711	-5.707	5.963	11.67
b_{n1}	Vein	-1.018[w]	1.198	-5.918	5.769	11.687
a_{n2}	Vein	-0.016	0.613	-3.797	3.731	7.528
b_{n2}	Vein	0.061[w]	0.597	-3.723	4.246	7.969

Descriptive statistics of the harmonic regression wave amplitude, the cosine and sine coefficients of the first and second harmonics of the two study groups. HRW_a = harmonic regression wave amplitude, $a_{n1,2}$ = Fourier cosine coefficient of the first and second harmonic, $b_{n1,2}$ = Fourier sine coefficient of the first and second harmonic, ICP_n = normal intracranial pressure group, ICP_h = high intracranial pressure group, IQR = interquartile range, Highlighted cells[w] = within group, Highlighted cells[b] = between group median differences failed to achieve statistical significance at a level $p<0.05$.

by a positive slope of regression with IOP_i, was 0.0051±0.00006 (p-value<0.00001). The corresponding values for the retinal arterial system were -0.028±0.0021, -0.0031±0.0004 and 0.0071 ±0.000065 (p-value<0.00001) respectively (Figs 3 and 4) in both plots there is attenuation of the HRW_a in the retinal venous system with increased distance along the vessel (V_{Dist}) and with increasing intracranial pressure (ICP). Amplification of the HRW_a with an increase in the induced intraocular pressure (IOP_i) is noted.

The equations of the regression lines for both the venous HRW_{a-YJtV}, and arterial HRW_{a-YJtA} can be derived:

$$HRW_{a-YJtV} = -0.0667 \cdot V_{Dist}(\pm 0.002) + 1.4823(\pm 0.04)$$

$$HRW_{a-YJtV} = 0.0051 \cdot IOP_i(\pm 0.00006) + 1.3156(\pm 0.04) \tag{1}$$

$$HRW_{a-YJtV} = -0.0059 \cdot ICP(\pm 0.0004) + 1.5472(\pm 0.04)$$

$$HRW_{a-YJtA} = -0.0282 \cdot V_{Dist}(\pm 0.0021) + 1.4564(\pm 0.05)$$

$$HRW_{a-YJtA} = 0.0071 \cdot IOP_i(\pm 0.00007) + 1.2746(\pm 0.05) \tag{2}$$

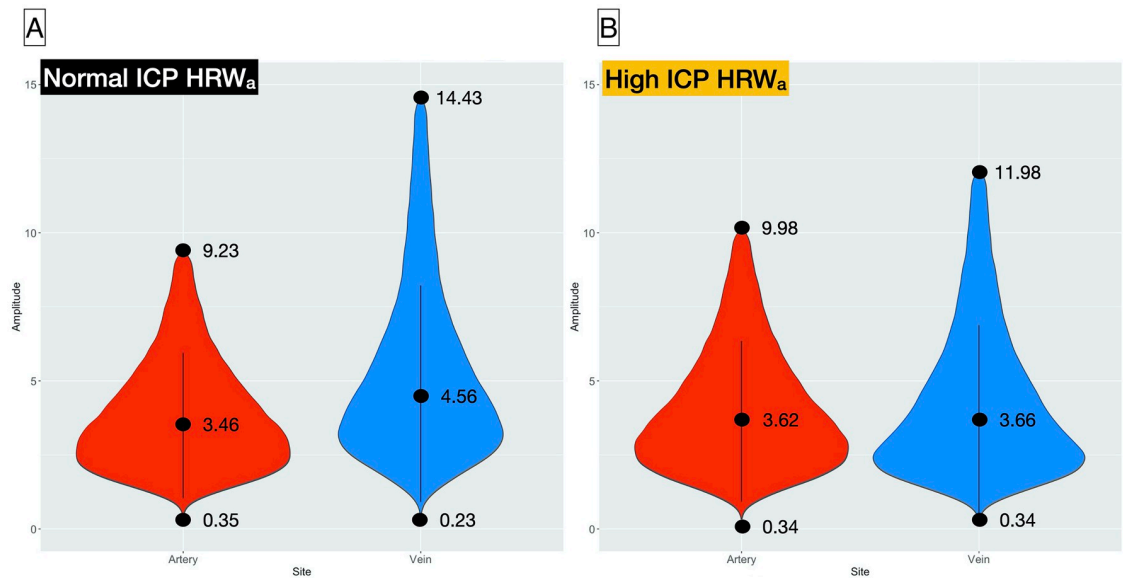$$HRW_{a-YJtA} = -0.0031 \cdot ICP(\pm 0.0004) + 1.4864(\pm 0.05)$$

Fig 2. Violin plot of the distribution of the HRW$_a$. A) Study group with normal intracranial pressure ICP$_n$ (ICP≤25cm water) and B) high intracranial pressure ICP$_h$ (ICP>25cm water). The median ± IQR (line and center dot) and range (end dots) are highlighted for each group.

Where the coefficients of all equations were highly statistically significant (p<0.00001). For both retinal vascular systems, the negative coefficients of V$_{Dist}$ and ICP indicate that decay in retinal venous pulsation amplitude in response to these predictors and a positive correlation with IOP$_i$. From Eqs (1) and (2), it can be noted that the retinal vascular pulse wave attenuation of the retinal veins is approximately two times that of the retinal arteries.

A graphical display of the interactions is demonstrated in Fig 5. They display the relationship between the dependent variable on the y-axis i.e. mean pulsation amplitude (HRW$_{a-YJt}$ and Fourier coefficients, which are the cosine (a$_n$) and sine (b$_n$)) and the independent variable on the x-axis i.e. vessel type (artery and vein), also called the main effect. This relationship is evaluated under different ICP levels grouped into two factor levels (high and normal). It is worth considering the specific terminology used when describing interaction plots, these pertain to two observations reported from these plots. The first if there is a main effect, this is present when the line connecting the mean pulsation amplitudes between two different vessel types is sloped, which indicates the difference in the mean pulsation amplitude between is statistically significant. The steeper the slope of the line, the greater the magnitude of the main effect. In contrast, a main effect is absent when the line connecting the mean pulsation amplitudes is horizontal and therefore parallel to the x-axis, in this state, there is no statistically significant difference in the mean pulsation amplitude between the artery and vein. The second observation is the presence of an interaction with the grouping factor (ICP), this may be disordinal when there is an intersection of the two lines connecting the means, or ordinal when the lines are non-parallel and non-intersecting [49].

From Fig 5, there is a significant main effect as a result of a statistically significant difference between the mean HRW$_a$ pulsation amplitudes between the vessels. Also, there is disordinal (cross-over) interaction between the two ICP groups. Noted are a high mean arterial and low mean venous HRW$_{a-YJt}$ pulsation amplitude in the ICP$_h$ group and conversely for the ICP$_n$ group. The a$_{n1}$ showed no interaction between the ICP groups, however, there was a
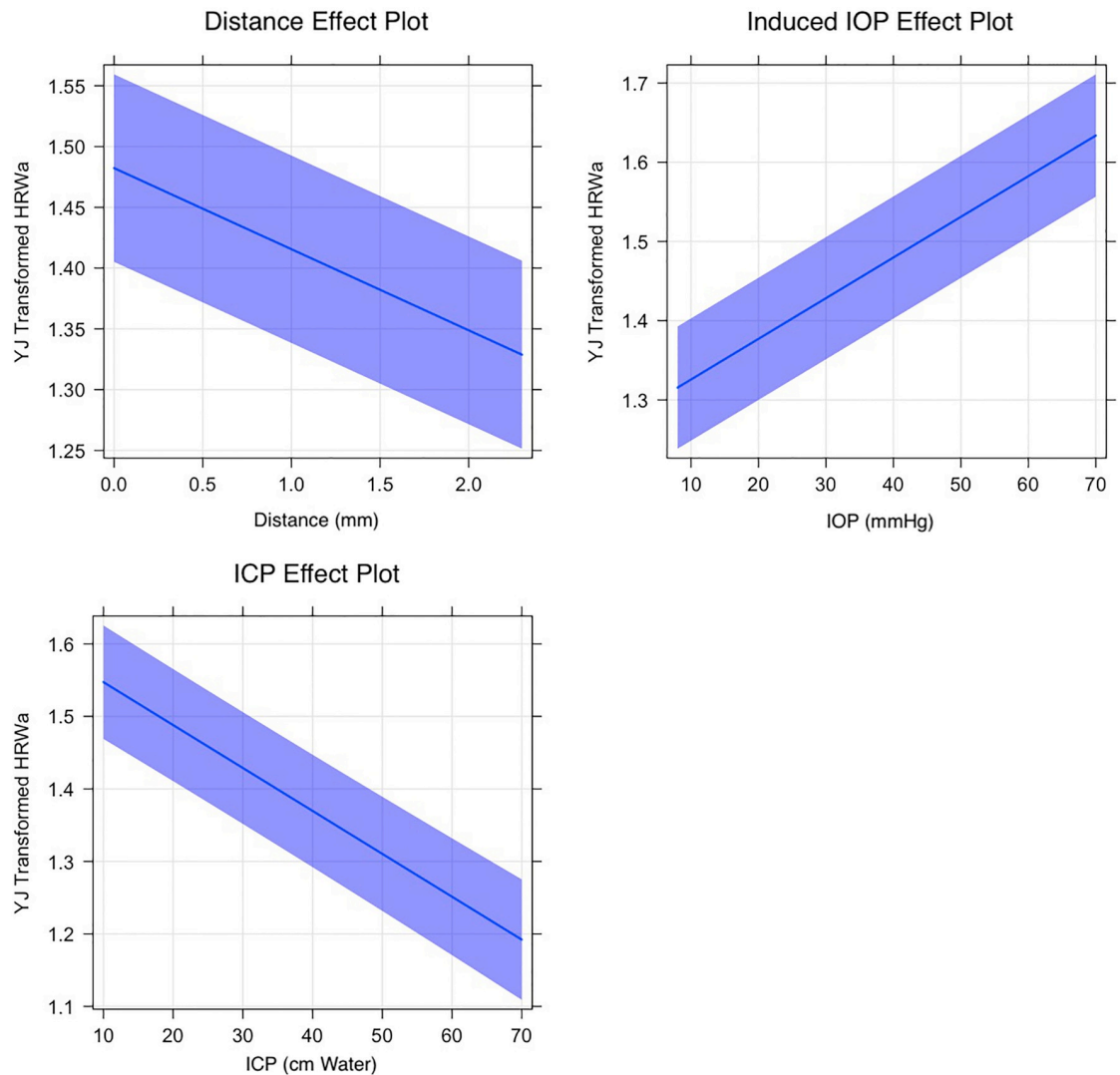
Fig 3. Effect plot of the retinal venous harmonic regression waveform amplitude (HRW$_a$). The slope of regression line correlating the HRW$_a$ with V$_{Dist}$ was -0.071±0.002 whereas that correlating with ICP was -0.0059±0.0004. There was amplification of the HRW$_a$ as indicated by a positive slope of regression with IOP$_i$, was 0.0051±0.00006 for all coefficients p-value<0.00001.

https://doi.org/10.1371/journal.pone.0270557.g003

significant main effect. Based on a lack of interaction with ICP, the coefficient follows the effect of the IOP wave, and therefore the effects of IOP$_i$ on the retinal vessel wall. The a$_{n2}$ showed ordinal (non-intersecting, non-parallel) interaction where between-group differences in the value of this coefficient existed only in the retinal veins (Fig 5). The interaction plots the sine (b$_{n1}$) coefficient show a strong interaction between ICP groups and the loss of main effects in the ICP$_h$ group as indicated by the parallel line joining the mean pulsation values to the x-axis. The sine (b$_{n2}$) coefficient showed ordinal interaction with ICP but there was a loss of a main effect in the ICP$_h$ group. Based on these observations the b$_{n1}$ and the second harmonic coefficients mirror the retinal vascular response to the ICP wave.

A mixed-effects linear regression hierarchal model was used to quantify the interactions between the predictors for the HRW$_{a-YJt}$, for the retinal veins (Fig 6) and arteries (Fig 7). Where HRW$_{a-YJt}$ is the Yeo-Johnson transformed value of the retinal vascular pulse, ICP is in
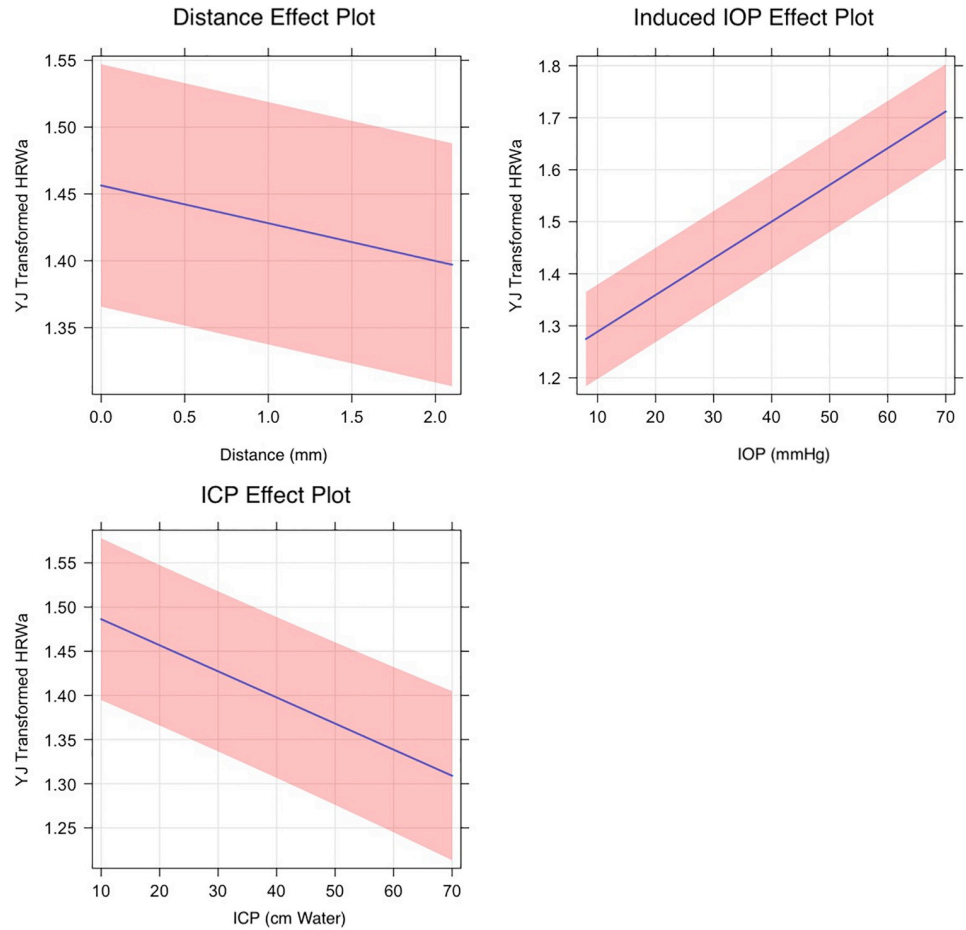
Fig 4. Effect plot of the retinal arterial harmonic regression waveform amplitude (HRW_a). The slope of regression line correlating the HRW_a with V_{Dist} was -0.028±0.0021 whereas that correlating with ICP was -0.0031±0.0004. There was amplification of the HRW_a as indicated by a positive slope of regression with IOP_i, was 0.0071±0.000065 for all coefficients p-value<0.00001.

https://doi.org/10.1371/journal.pone.0270557.g004

cm water, IOP_i is the induced IOP in mmHg, and V_{Dist} is in mm from the center of the optic disc:

$$
\begin{aligned}
HRW_{a-YJtV} = &-0.3638(\pm 0.013) \cdot V_{Dist} + 0.00091(\pm 0.00029) \cdot IOP_i \\
&-0.01149(\pm 0.00052) \cdot ICP + 0.0071(\pm 0.00036) \cdot V_{Dist} \cdot IOP_i \\
&+0.0085(\pm 0.00041) \cdot V_{Dist} \cdot ICP + 0.000094(\pm 0.0000093) \cdot IOP_i \cdot ICP \\
&-0.0001612(\pm 0.000012) V_{Dist} \cdot IOP_i \cdot ICP + 1.69
\end{aligned}
\tag{3}
$$

$$
\begin{aligned}
HRW_{a-YJtA} = &-0.2374(\pm 0.017) \cdot V_{Dist} + -0.00038(\pm 0.00038) \cdot IOP_i \\
&-0.00708(\pm 0.00057) \cdot ICP + 0.0089(\pm 0.00053) \cdot V_{Dist} \cdot IOP_i \\
&+0.00376(\pm 0.00059) \cdot V_{Dist} \cdot ICP + 0.000188(\pm 0.000013) \cdot IOP_i \cdot ICP \\
&-0.0002(\pm 0.000018) V_{Dist} \cdot IOP_i \cdot ICP + 1.50
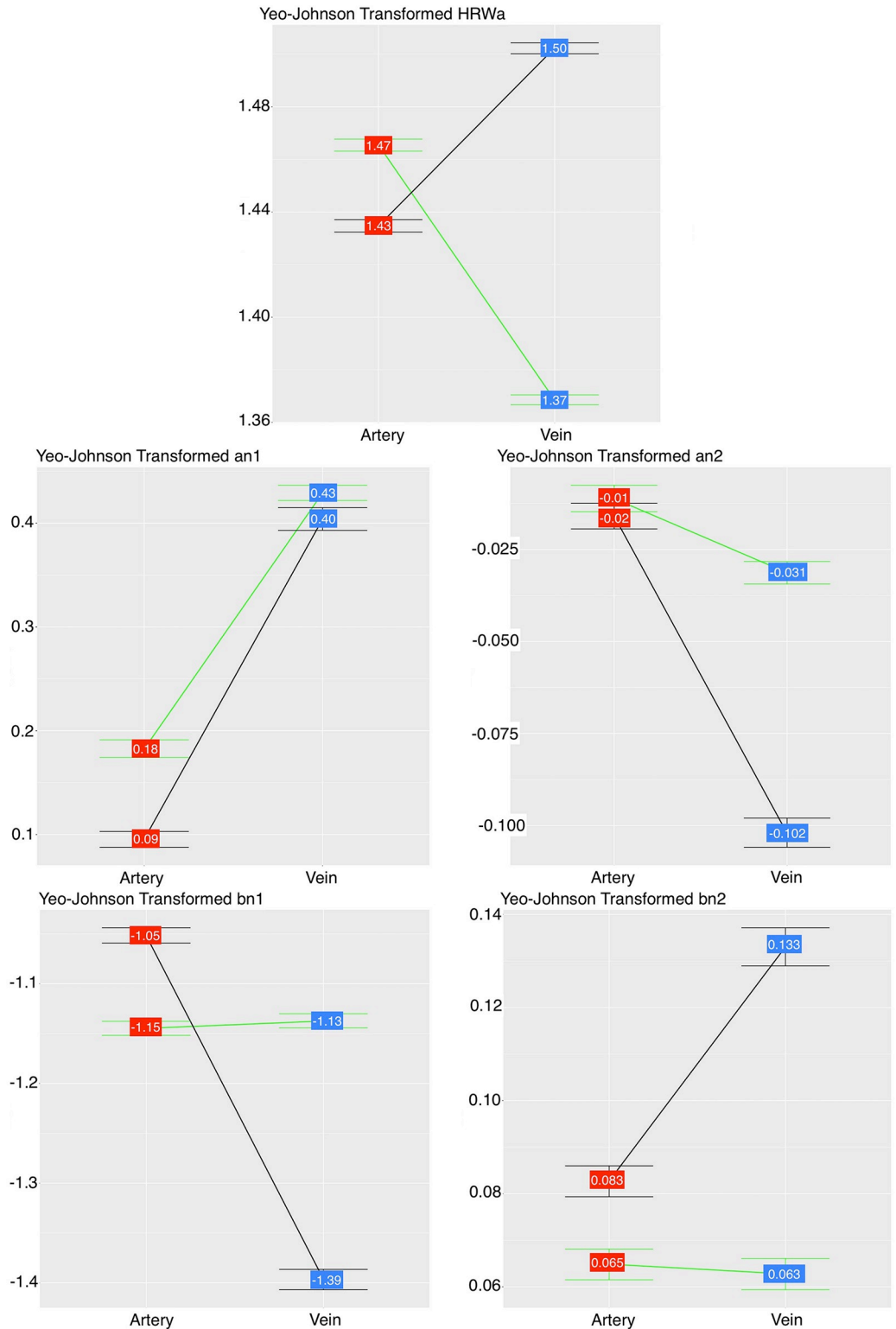\end{aligned}
\tag{4}
$$

Fig 5. Interaction plot of the harmonic regression waveform amplitude (HRW$_a$), cosine (a$_{n1,2}$) and sine (b$_{n1,2}$) coefficients of the first and second harmonics. In both the high (h) and normal (n) intracranial pressure groups for both vascular systems there was interaction of the HRW$_a$ and b$_{n1}$, no interaction of the a$_{n1}$ term and ordinal interaction of the a$_{n2}$ and b$_{n2}$ terms. Therefore the sine coefficient (b$_{n1}$) and the second harmonic coefficients reflects the retinal vascular pulse response to ICP and the cosine coefficient (a$_{n1}$) follows the IOP pulse wave response on the vessel wall. Color code: green = ICP$_h$, black = ICP$_n$ study group.

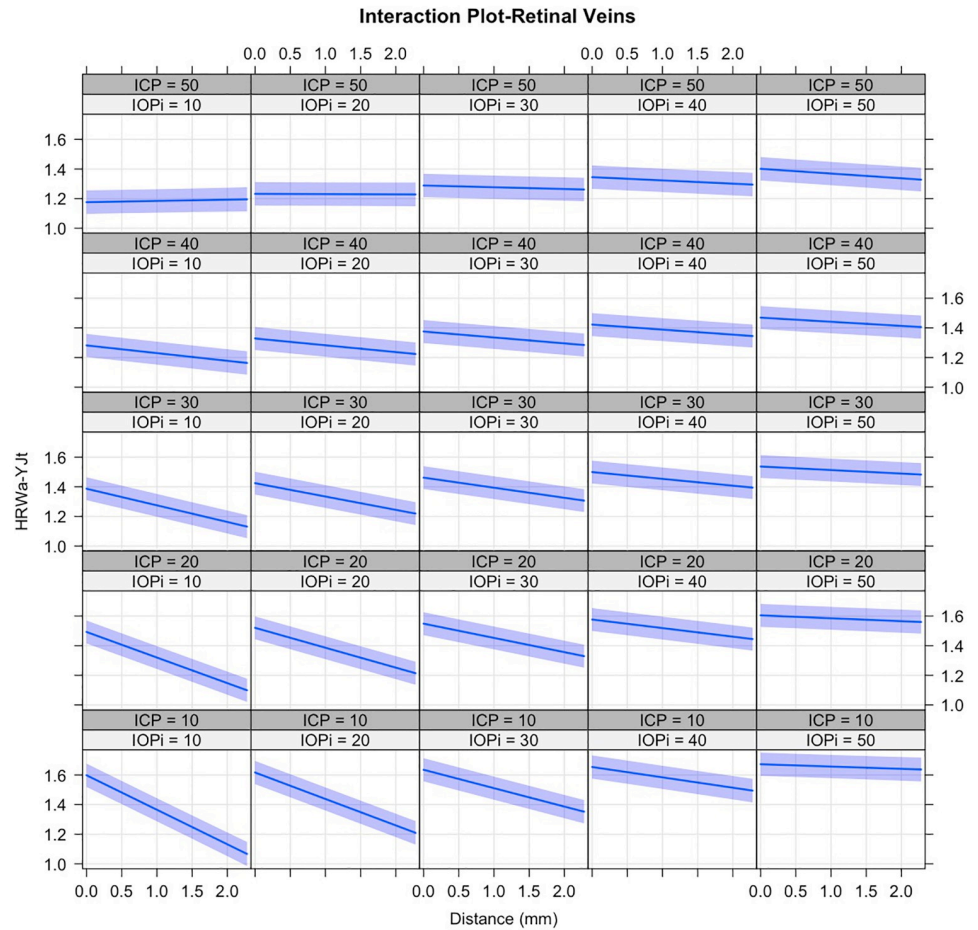https://doi.org/10.1371/journal.pone.0270557.g005

Fig 6. Trellis graph demonstrating the mixed effects linear regression model with interactions of the Yeo-Johnson transformed venous harmonic regression waveform amplitude (HRW$_{a\text{-YJt}}$). Distance is measured in millimeters (mm) from the center of the optic disc. The 95% confidence intervals are shown around the regression lines. Noted is a reduction of the slope of the regression with increased ICP (columns) and IOP$_i$ (rows). Whereas the y-intercepts of the regression lines are reduced with increased ICP, they are increased with higher IOP$_i$. The progressively lower y-intercepts of the regression lines along the lower left to upper right diagonal indicate that a higher IOP$_i$ is required to induce a venous pulsation with higher ICP, which will be of a lower amplitude.

https://doi.org/10.1371/journal.pone.0270557.g006

Both equations can be rearranged in terms of V$_{Dist}$, which allows some interaction terms to be eliminated:

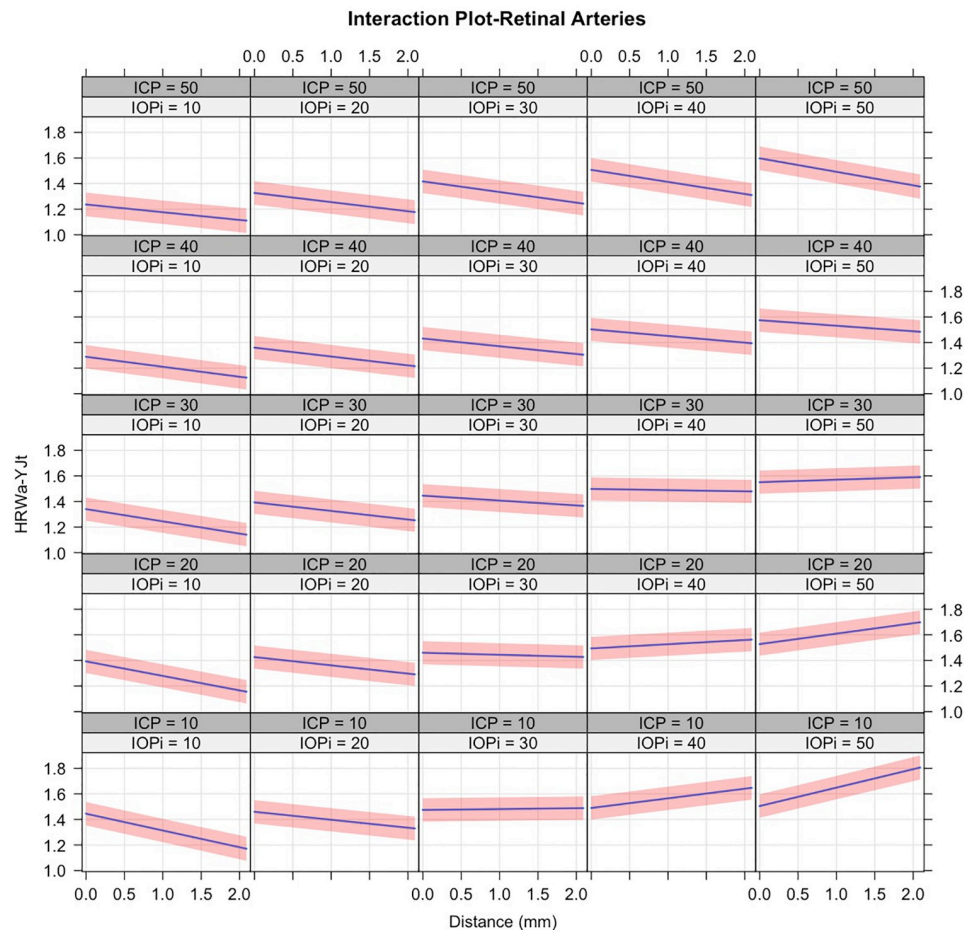| **Harmonic Regression Waveform Amplitude-Venous** |
|:---:|
| $HRW_{YJt-V} = +1.6943862 + V_{Dist} \cdot [-0.3638445 + 0.0070505 \cdot IOP_i + 0.0076471 \cdot ICP$ $-0.0001612 \cdot IOP_i \cdot ICP] + 0.0009149 \cdot IOP_i - 0.0114921 \cdot ICP + 0.0000943 \cdot IOP_i \cdot ICP$ |
| **Harmonic Regression Waveform Amplitude-Arteria** |
| $HRW_{YJt-A} = +1.5004466 + V_{Dist} \cdot [-0.2373716 + 0.0088757 \cdot IOP_i + 0.0037635 \cdot ICP$ $-0.0002001 \cdot IOP_i \cdot ICP] - 0.0003786 \cdot IOP_i - 0.0070824 \cdot ICP + 0.0001880 \cdot IOP_i \cdot ICP$ |

Fig 7. Trellis graph demonstrating the mixed effects linear regression model with interactions of the Yeo-Johnson transformed arterial harmonic regression waveform amplitude (HRW$_{a-YJt}$). Distance is measured in millimeters (mm) from the center of the optic disc. The 95% confidence intervals are shown around the regression lines. Noted is a increase of the slope of the regression with increased ICP (columns) and IOP$_i$ (rows) particularly with ICP in the pathological range. Contrary to the retinal veins the progressively higher y-intercepts of the regression lines along the lower left to upper right diagonal indicate that amplification of the retinal arterial pulsation occurs with a higher ICP. A reversal of the slope of the regression at ICP 10–20 at an IOP$_i$ >30 mmHg is seen, this is likely a spurious result as a consequence of the boundary conditions of the mixed effects linear model.

https://doi.org/10.1371/journal.pone.0270557.g007

The interactions are displayed graphically in Figs 6 and 7.

All coefficients of the regression equations with interactions achieved statistical significance (p<0.001), except the arterial IOP$_i$ coefficient (p = 0.32). The overall interaction model predicting the HRW$_{a-YJtV}$ had a total explanatory power (conditional R^2) of 38.7%, in which the fixed effects explained 8.8% of the variance (marginal R^2). Within this model the effect of V$_{Dist}$ and ICP were significant ($\beta_{V_{Dist}} = -0.42$, se = ±0.015, p < 0.00001) and (β_{ICP} = -0.42, se = ±0.019, p < 0.00001). Whereas that for IOP$_i$ was small ($\beta_{IOP_i} = 0.031$, se = ±0.0097, p < 0.00001).

It can be observed from Fig 6 that there is a reduction of the slope of the regression line with increased ICP (columns) and IOP$_i$ (rows). Whereas the intercept of the regression lines are reduced with increased ICP, observed as a progressive reduction in venous pulsation, the converse occurs with raised IOP$_i$. Following a diagonal of the trellis graph (Fig 6) from the

lower left to the upper right, where both ICP and IOP_i increase, it can be observed that a higher IOP_i is required to induce venous pulsations of progressively lower amplitude in the presence of a higher ICP. The interactions in the retinal arteries seen in (Fig 7) depend on whether ICP is pathologic or physiologic. Where ICP is pathological, the intercept of the regression lines are is increased with increased IOP_i. At the physiologic ICP range, there is an increase in the intercept therefore an increase in retinal arterial pulse amplitude with increasing IOP_i, however, this increase in intercept is less than that in the pathological ICP range. A reversal of the slope of the regression at ICP 10–20 at an IOPi >30 mmHg is seen. This is likely a spurious result as a consequence of the boundary conditions of the mixed-effects linear model. Contrary to the retinal veins when a diagonal of the trellis graph (Fig 7), followed from the lower left to the upper right, where both ICP and IOP_i increase, a corresponding increase in retinal arterial pulse amplitude can be observed.

The overall interaction model predicting the HRW_{a-YJtA} has a total explanatory power (conditional R^2) of 42%, in which the fixed effects explained 5.8% of the variance (marginal R^2). Within this model the effect of V_{Dist} and ICP were significant ($\beta_{V_{Dist}} = -0.26$, se = ±0.019, p < 0.00001) and (β_{ICP} = -0.21, se = ±0.017, p < 0.00001). Whereas that for IOP_i was small and did not achieve statistical significance ($\beta_{IOP_i} = -0.013$, se = ±0.013, p < 0.32).

The statistical significance of the coefficients of the linear regression model with interactions of the HRW_{a-YJt} and the terms of the Fourier series are summarised in Table 3.

Discussion

We quantified the difference between retinal venous and arterial pulse amplitudes in subjects with high and normal intracranial pressures over a range of induced intraocular pressures, which demonstrated a reduction in retinal venous and an increase in arterial pulsation amplitudes with raised ICP. In our current study both the fixed effects and the random factors in the

Table 3. Estimated interaction model coefficients.

	HRW_a	a_{n1}	b_{n1}	a_{n2}	b_{n2}
Artery					
V_{Dist}	-0.237±0.017	-0.193±0.05171	0.3681±0.0551	0.2315±0.028	-0.1451±0.0303
IOP_i	-0.00038±0.00038*	0.0084±0.00113	-0.01155±0.0012	-0.00228±0.00061	-0.0047±0.00066
ICP	-0.0071±0.00057	-0.0073±0.0017	0.02934±0.0018	0.0069±0.00091	-0.0248±0.00099
$V_{Dist} \cdot IOP_i$	0.0089±0.00053	-0.0155±0.0016	-0.0042±0.00167	0.00051±0.00084*	0.0041±0.00091
$V_{Dist} \cdot ICP$	0.0037635±0.00059	0.00221±0.0018*	-0.0049±0.0019	-0.00624±0.00095	0.00094±0.001035*
$IOP_i \cdot ICP$	0.0001880±0.000013	0.00013±0.000039	-0.000156±0.000041	0.000088±0.000021	0.00015±0.000023
$V_{Dist} \cdot IOP_i \cdot ICP$	-0.0002±0.000018	0.000267±0.000053	0.000124±0.000056	0.00001±0.000029*	-0.000013±0.000031*
Vein					
V_{Dist}	-0.3638±0.013	-0.0847±0.051*	-0.5504±0.0541	-0.0431±0.0242*	-0.1225±0.0254
IOP_i	0.00091±0.00029	0.0232±0.0011	-0.048±0.0012	-0.0032±0.00054	-0.000195±0.00056*
ICP	-0.0115±0.00052	0.0181±0.0020	0.0031±0.0022*	0.01795±0.00097	-0.00682±0.001
$V_{Dist} \cdot IOP_i$	0.0071±0.00036	-0.0083±0.0014	0.0395±0.0015	0.00156±0.00067	0.001±0.0007*
$V_{Dist} \cdot ICP$	0.0076±0.00041	-0.0026±0.0016*	0.0271±0.00173	-0.00092±0.00077*	-0.00184±0.00081
$IOP_i \cdot ICP$	0.000094±0.0000093	-0.00023±0.000036	0.0011±0.00004	-0.000013±0.000018*	-0.00012±0.000018
$V_{Dist} \cdot IOP_i \cdot ICP$	-0.00016±0.000011	0.00019±0.000041	-0.0011±0.000045	0.000023±0.00002*	0.000088±0.000021

Estimated interaction model coefficients of the terms of the first two harmonics of the Fourier series. CS = computationally singular. Highlighted cells (*) represent coefficients that failed to achieve statistical significance. p-value<0.001 for the rest of the coefficients.

linear models accounted for approximately 40% and the predictors accounted for less than 10% of the variance in the study population, despite the linear models' coefficients achieving a high level of statistical significance the variance between individuals (heteroscedasticity) in the vascular pulsation amplitudes precludes the use of the model as a predictor of ICP. However, the interpretive nature of the linear models allowed further analysis of the retinal vascular responses to a range of ICP values.

One of the significant findings was the reduction in the median venous and the increase in the median arterial HRW_a in the ICP_h group (Fig 2). Spontaneous venous pulsation (SVP) is a result of the pressure gradient along the retinal vein as it traverses the lamina cribrosa. Loss of spontaneous venous pulsation is a recognized sign of increased ICP [50, 51], as increase in ICP increases intracranial pulse pressure. Consequently, SVP ceases when the ICP pulse pressure is equal to intraocular pulse pressure [52]. Although SVPs are classically described as a categorical and binary clinical sign, in this work and previous reports we demonstrated that modified photoplethysmography can provide a quantitative measure of this clinical sign non-invasively [29, 50]. Whereas changes in the retinal venous system with high ICP have been described in the literature, where a reduction in retinal venous compliance occurs from the combined influence of increased intravenous pressure, venous distension, and increase in venous wall tension [5, 7, 53, 54]. The literature has been less definite on the changes in the retinal arterial circulation, Querfurth and Mitrra et al. reported a reduction in retinal arterial flow velocities in mild to moderate raised ICP [55]. Querfurth found a paradoxical increase in central retinal and the ophthalmic arterial flow velocities with an ICP $\geq$450 mm water [56]. Other sonographic studies reported an increase in pulsatility index of the central retinal artery regardless of ICP levels [2, 57]. Interpretations of the vascular response remain hypothetical. Modified Photoplethysmography cannot inform why differences in pulsation patterns exist between the vessels in the two study groups.

Differences between the retinal arterial and venous pulsation amplitude, patterns, and attenuation distance arise from unique properties of the pressure-flow wave, resistance, and vessel wall structural characteristics. Consequently, a range of reported prevalences of detectable retinal vascular pulsation is dependent on the measurement methodology. Clinically observable spontaneous retinal venous pulsations are reported in 67% to 98% of normal eyes [19, 51, 58, 59], compared to the arterial pulse where spontaneous pulsations have been reported to be physiologically absent and only associated with vascular pathology [60–62]. As an extension of clinical observation, modern imaging technology has facilitated the detection and measurement of retinal vascular pulsations and has rendered the arterial pulse measurable physiologically. Clinically available methods include: dynamic fluorescein [63] and indocyanine angiography [64, 65], near-infrared reflectance ophthalmoscopy [59], swept-source optical coherence tomography [66], adaptive optics imaging [67], and the Dynamic Vessel Analyzer [68]. In the largest study to date, McHugh et al. reported the detectability of spontaneous retinal venous pulsation in a normal population using near-infra-red videography. Their cross-sectional study design was conducted on 105 patients with presumed normal intracranial pressure, spontaneous venous pulsation was detected in 97% to 100% of subjects [69]. Whereas this study investigated the detectability of retinal venous pulsation, the prevalence of retinal arterial pulsations was not reported. Using the same technology, Moret et al., used principal component analysis to filter videos of the optic nerve and temporal peripapillary area. They reported a low detection rate as they observed spontaneous venous pulsation in 5 of 10 (50%) subjects. This was likely due to the low device frame rate of 9 frames per second used in their study. However, they reported various arterial pulsation patterns including the serpentine movement of the principal arteries, pulsatile vessels of the optic nerve head, vessel displacement, and arterio-venous mechanical coupling [59]. Modified Photoplethysmography,

distinct from other technologies, quantifies the retinal vascular pulse amplitude in the Fourier domain. This method has been validated in previous work [29, 31, 43, 50] where we reported quantifiable differences in the normal retinal vessel pulsations. In a study on 28 eyes of 16 normal subjects, we reported the normal median venous pulse amplitude was approximately 1.5 times and the rate of decay was twice that of the arterial pulse wave [29]. Similarly, in the current study the venous pulse amplitude was 1.3 times and the coefficient of decay 2.3 times that of the arterial. Therefore physiological properties account for differences in pulse amplitude differences between the arteries and the veins. From the weighted β coefficients of linear models with interactions (Eqs (3) and (4)) it is noted that both V_{Dist} and ICP have a similar damping effect on venous wall ($\beta_{V_{Dist}} = -0.42$, se = ±0.015, β_{ICP} = -0.42, se = ±0.019, p < 0.00001). As described above, reduction in venous wall compliance as a result of venous distension accounts for this effect, the damping effect of ICP on the arterial wall is less than V_{Dist} ($\beta_{V_{Dist}} = -0.26$, se = ±0.019, β_{ICP} = -0.21, se = ±0.017, p < 0.00001), both structural differences of different vessel types may account for differences in pulsation decay rates.

In previous work, we quantified the decay in the retinal vascular pulse amplitude from a population of healthy subjects and reported that although the amplitude of the retinal venous pulse is higher it decays over a shorter distance compared to that of the arterial [29]. Differences in attenuation and amplification in retinal vascular pulse between the retinal arteries and veins in response to V_{Dist}, ICP and IOP_i (Figs 3 and 4) are due to variations in retinal vascular compliance and resistance. Whereas systemic arterial compliance plots are curvilinear, this relationship is sigmoidal in the veins, resulting in a 19 to 24 times difference in systemic venous compliance for an equivalent transmural pressure and cross-sectional area [70–75]. This relationship has not been quantified directly in the retinal vascular system, however, among the many structural differences, including differences in collagen content, the thinner venous wall consists of a muscle layer that is 3–4 layers thick compared to the 5–7 layers found in the artery [76] indicates the lower compliance in this part of the vascular tree. Resistance to hemodynamic flow is set by circulating blood, net length, branching pattern, and cross-sectional area of the specific circulation. Similar to the systemic circulation, the primary site of resistance resides in the small arteries and arterioles. However, unique to the ocular circulation, the retinal vein, which is the low resistance part of the retinal circulation, is subject to an external compression force in the form of intraocular pressure, thereby acting as a Starling resistor, which is defined as a mechanism that maintains constant flow through a collapsible tube when the latter is surrounded by varying pressure and contained in a pressurized chamber, the mechanisms and significance of which remains unknown [77–79]. Theoretically, both compliance and resistance are dependent on tension (T) in the vessel wall, which according to Laplace's law [80], is proportional to the product of the blood vessel radius (r) and transmural pressure (P_{tm}, defined as the difference between intra-luminal and extra-luminal pressures)

$$T = P_{tm} \cdot r$$

For pulsations to occur in a vessel segment, either a pressure gradient must exist or the transmural pressure must be reduced to overcome this mural tension. Both IOP_i and ICP influence the mural tension. The retinal veins are more susceptible than arteries to changes in IOP_i and ICP due to the thinner walls, wider radius, lower intraluminal pressure, and hence lower resistance in the veins compared to the arteries. There are two mechanisms by which ICP and IOP_i can influence wall tension and therefore the retinal vascular pulse:

1. Reduction in transmural pressure: The lower limit for retinal venous pressure is determined by the ocular perfusion pressure, which is the difference between mean arterial pressure and IOP_i, therefore the central retinal venous pressure must exceed IOP_i to prevent venous

wall collapse [81]. The lower limit in the retinal arterial pressure is the diastolic pressure [82, 83]. As IOP_i rises, transmural pressure decreases, resulting in an increase in vessel wall compliance through lowering wall tension. The vessel collapses partially or completely during a period of the cardiac cycle when the transmural pressure is between diastolic and systolic intra-luminal retinal vascular pressure (within the pulse pressure range). As systolic pressure exceeds the transmural pressure, the vessel re-fills, producing vascular pulsations. [60, 84]. When transmural pressure is negative, the vessel wall collapses, and pulsations in the vascular segment cease. Because the collapse pressure in the retinal veins is lower than in the retinal arteries, a higher the transmural pressure range (and hence higher IOP_i) influences the thicker-walled arteries after venous wall collapse occurs, which may explain the different IOP_i ranges to induce pulsations in the retinal veins and arteries.

2. Reduction in retinal venous compliance: The effect of raised ICP on the retinal circulation is to increase resistance in the venous circulation [62] combined with reduced venous compliance due to vessel wall distension [71, 85]. The mechanism for increased retinal arterial pulsations, in this case, remain unclear. However, analogous to the observation of arteriolar pulsations reported in type A central retinal vein occlusion characterized by pulsatile arterial filling [62], possible mechanisms include:

    1. Elevated IOP_i above central retinal arterial diastolic pressure as hypothesized with pulsations of the central retinal artery occurring due to ophthalmodynamometry [82, 83]. Together with reduced venous compliance of the artery wall, may limit the damping of the vascular pulse pressure, resulting in increased arterial pulsations proportional to elevated ICP [86].

    2. Augmentation of the vascular pressure wave through wave reflections and possibly widening of the retinal vascular pulse pressure. Although this mechanism has not been demonstrated in the retinal vessels, wave reflections are ubiquitous throughout the circulation, particularly at sites of higher input impedance. Impedance is a complex value frequency domain parameter with both magnitude and phase, it indicates alterations in compliance, resistance, and inertance. Mismatching vascular impedances reduces the pulse transmission efficiency for the propagating pulse towards the venous side of the circulation, consequently wave reflections arise, which augment the pressure wave amplitude and reduce flow due to phase differences [34, 36, 87, 88].

We hypothesize these mechanisms could explain the changes with the pulsation amplitudes in Figs 6 and 7, where ICP and IOP_i have different influences on the retinal vascular pulse, primarily through the venous side of the circulation due to the thinner wall, lower resistance, and higher compliance.

We did not evaluate the spectral properties of the IOP nor the ICP wave in our study. However, the interaction plots (Fig 5), which compare the pulsation amplitude between the two study groups, suggest a that the Fourier coefficients convey information from the vessel walls, where the cosine (a_{n1}) and sine coefficient (b_{n1}) mirror the effects of IOP_i, and the ICP wave, respectfully. Other investigators reported on the spectral properties of the latter two pressure waves, Evans et al. analyzed the IOP pulse's higher spectral components up to the fourth harmonic and Bozic et al. compared the spectral components of the IOP pulse wave up to the fifth harmonic, however, the hemodynamic significance of the Fourier analysis remains obscure [89–91]. Takizawa et al., in an experimental study, described the frequency spectrum and amplitude transfer function at different locations in the craniospinal axis, they concluded that the ICP pulse waveform is almost the same at any location in the intracranial space and the origin of the ICP pulse wave is the pulsation of the brain parenchyma derived from cerebral

arterial blood flow [92]. None of these studies specifically identified Fourier coefficients associated with these pressure waves, our results may guide future predictive modeling for non-invasive estimation of ICP. The accessibility of the retinal vasculature makes it a favorable means of non-invasive prediction of ICP. Additionally, a particularly strong association between retinal and intracranial pathology arises from the common embryonic origin shared between the retina and the brain, consequently, both animal and experimental evidence demonstrate similarities in circulatory physiology [93]. During embryonic development, the retina and optic nerve extend from the diencephalon, and are thus considered part of the central nervous system [94]. They possess similar structural and functional features such as autoregulation, a blood-retina barrier, and glial cell connections [94–97]. Non-invasive ICP prediction would not only reduce the risks of invasive procedures, but it would provide an accessible avenue to explore neuro-ophthalmic, retinal vascular, and glaucomatous optic neuropathy and perhaps provide further insight into the pathogenesis of these disorders.

In summary, the retinal vascular changes are a consequence of a complex interaction between the retinal hemodynamics (retinal pressure-flow wave and vessel wall), IOP, ICP, and systemic blood pressure, in addition to biomechanical properties of the lamina cribrosa [1, 5, 54, 98]. In pathological ICP ranges, whereas the retinal venous pulsation amplitude is reduced due to decreased wall compliance and venous distension, the retinal arteries demonstrate an increase in pulse amplitude. Mechanisms in the arteries remain hypothetical. However, possible mechanisms include a reduction in damping of the arterial pulse pressure, augmentation of the arterial pressure wave through wave reflections, and widening of the retinal arterial pulse pressure. Although both are generated by the cardiac cycle, the influence of IOP and ICP pressure waves on the vessel wall might be evaluated by separate Fourier coefficients.

Limitations of our study include the limited number of subjects and the lack of simultaneous blood pressure measurements, which may have assisted in the interpretation of the findings in the retinal arterial system.

Conclusion

The retinal vascular pulsation characteristics in the ICP_h group showed high retinal arterial and low venous pulsation amplitudes. Interactions between retinal vascular pulsation amplitude and ICP suggest that the Fourier sine coefficient b_{n1} reflects the retinal vascular response to the ICP wave. Although a matrix of regression lines showed high linear characteristics, the low model explanatory power precludes its use as a predictor of ICP. These results may guide future predictive modelling in non-invasive estimation of ICP using modified photoplethysmography.

Supporting information

S1 Data.
(CSV)

Author Contributions

Conceptualization: Anmar Abdul-Rahman, William Morgan, Ying Jo Khoo, Christopher Lind, Allan Kermode, William Carroll, Dao-Yi Yu.

Data curation: Anmar Abdul-Rahman, William Morgan, Ying Jo Khoo, Christopher Lind, Allan Kermode, William Carroll, Dao-Yi Yu.

Formal analysis: Anmar Abdul-Rahman.

Investigation: Anmar Abdul-Rahman, William Morgan, Christopher Lind, Allan Kermode, William Carroll, Dao-Yi Yu.

Methodology: Anmar Abdul-Rahman, William Morgan, Christopher Lind, Allan Kermode, William Carroll, Dao-Yi Yu.

Project administration: Ying Jo Khoo, Dao-Yi Yu.

Resources: Anmar Abdul-Rahman, Ying Jo Khoo.

Software: Anmar Abdul-Rahman, William Morgan.

Supervision: William Morgan, Dao-Yi Yu.

Validation: Anmar Abdul-Rahman, William Morgan.

Visualization: Anmar Abdul-Rahman, William Morgan.

Writing – original draft: Anmar Abdul-Rahman.

Writing – review & editing: Anmar Abdul-Rahman, William Morgan, Allan Kermode, William Carroll, Dao-Yi Yu.

References

1. Rios-Montenegro EN, Anderson DR, David NJ. Intracranial pressure and ocular hemodynamics. Arch Ophthalmol. 1973; 89(1):52–58. https://doi.org/10.1001/archopht.1973.01000040054013 PMID: 4630889

2. Jeub M, Schlapakow E, Ratz M, Kindler C, Schievelkamp AH, Wabbels B, et al. Sonographic assessment of the optic nerve and the central retinal artery in idiopathic intracranial hypertension. Journal of Clinical Neuroscience. 2020; 72:292–297. https://doi.org/10.1016/j.jocn.2019.09.003 PMID: 31540860

3. Canac N, Jalaleddini K, Thorpe SG, Thibeault CM, Hamilton RB. Pathophysiology of intracranial hypertension and noninvasive intracranial pressure monitoring. Fluids and Barriers of the CNS. 2020; 17 (1):1–21. https://doi.org/10.1186/s12987-020-00201-8 PMID: 32576216

4. Silverman A, Petersen NH. Physiology, Cerebral Autoregulation. 2020;.

5. Hayreh SS, Edwards J. Ophthalmic arterial and venous pressures. Effects of acute intracranial hypertension. The British journal of ophthalmology. 1971; 55(10):649. https://doi.org/10.1136/bjo.55.10.649 PMID: 5124843

6. Gibbs FA. Relationship between the pressure in the veins on the nerve head and the cerebrospinal fluid pressure. Archives of Neurology & Psychiatry. 1936; 35(2):292–295. https://doi.org/10.1001/archneurpsyc.1936.02260020086006

7. Ghate D, Kedar S, Havens S, Fan S, Thorell W, Nelson C, et al. The Effects of Acute Intracranial Pressure Changes on the Episcleral Venous Pressure, Retinal Vein Diameter and Intraocular Pressure in a Pig Model. Current Eye Research. 2020; p. 1–8.

8. Motschmann M, Müller C, Kuchenbecker J, Walter S, Schmitz K, Schütze M, et al. Ophthalmodynamometry: a reliable method for measuring intracranial pressure. Strabismus. 2001; 9(1):13–16. https://doi.org/10.1076/stra.9.1.13.711 PMID: 11262696

9. Querfurth HW, Arms SW, Lichy CM, Irwin WT, Steiner T. Prediction of intracranial pressure from noninvasive transocular venous and arterial hemodynamic measurements. Neurocrit Care. 2004; 1(2):183–194. https://doi.org/10.1385/NCC:1:2:183 PMID: 16174913

10. Baurmann M. Weitere Ergebnisse der intrakraniellen Druckmessung mit Hilfe der Netzhautvenenpuls-Beobachtung. Ber Dtsch Ophthalmol Ges. 1927; 46:96–117.

11. Berens C, Smith HT, Cornwall LH. Changes in the fundus and in the blood pressure in the retinal arteries in increased intracranial pressure: papilledema and optic atrophy. Archives of Neurology & Psychiatry. 1928; 20(6):1151–1171. https://doi.org/10.1001/archneurpsyc.1928.02210180002001

12. Raykin J, Samuels B, Feola A, Ethier R. Cerebrospinal fluid pressure and the translaminar pressure gradient in optic nerve head biomechanics. In: Roberts CJ, Dupps WJ, Downs JC, editors. Biomechanics of the Eye. Kugler Publications; 2018.

13. Jonas JB, Wang N, Nangia V. Ocular perfusion pressure vs estimated trans–lamina cribrosa pressure difference in glaucoma: the Central India Eye and Medical Study (An American Ophthalmological Society Thesis). Transactions of the American Ophthalmological Society. 2015; 113.

14. Berdahl JP, Fautsch MP, Stinnett SS, Allingham RR. Intracranial pressure in primary open angle glaucoma, normal tension glaucoma, and ocular hypertension: a case–control study. Investigative ophthalmology & visual science. 2008; 49(12):5412–5418. https://doi.org/10.1167/iovs.08-2228 PMID: 18719086

15. Ren R, Jonas JB, Tian G, Zhen Y, Ma K, Li S, et al. Cerebrospinal fluid pressure in glaucoma: a prospective study. Ophthalmology. 2010; 117(2):259–266. https://doi.org/10.1016/j.ophtha.2009.06.058 PMID: 19969367

16. Siaudvytyte L, Januleviciene I, Ragauskas A, Bartusis L, Meiliuniene I, Siesky B, et al. The difference in translaminar pressure gradient and neuroretinal rim area in glaucoma and healthy subjects. Journal of ophthalmology. 2014; 2014. https://doi.org/10.1155/2014/937360 PMID: 24876948

17. Walsh TJ, Garden JW, Gallagher B. Obliteration of retinal venous pulsations: During elevation of cerebrospinal-fluid pressure. Am J Ophthalmol. 1969; 67(6):954–956. https://doi.org/10.1016/0002-9394(69)90094-4 PMID: 5785858

18. Kahn E, Cherry G. The clinical importance of spontaneous retinal venous pulsation. Medical bulletin (Ann Arbor, Mich). 1950; 16(10):305–308. PMID: 14782335

19. Levin BE. The clinical significance of spontaneous pulsations of the retinal vein. Arch Neurol. 1978; 35 (1):37–40. https://doi.org/10.1001/archneur.1978.00500250041009 PMID: 619871

20. Rosenberg JB, Shiloh AL, Savel RH, Eisen LA. Non-invasive methods of estimating intracranial pressure. Neurocritical care. 2011; 15(3):599–608. https://doi.org/10.1007/s12028-011-9545-4 PMID: 21519957

21. Zhang X, Medow JE, Iskandar BJ, Wang F, Shokoueinejad M, Koueik J, et al. Invasive and noninvasive means of measuring intracranial pressure: a review. Physiological measurement. 2017; 38(8):R143. https://doi.org/10.1088/1361-6579/aa7256 PMID: 28489610

22. Khan MN, Shallwani H, Khan MU, Shamim MS. Noninvasive monitoring intracranial pressure–A review of available modalities. Surg Neurol Int. 2017; 8. https://doi.org/10.4103/sni.sni_403_16 PMID: 28480113

23. Czosnyka M, Pickard JD. Monitoring and interpretation of intracranial pressure. Journal of Neurology, Neurosurgery & Psychiatry. 2004; 75(6):813–821. https://doi.org/10.1136/jnnp.2003.033126 PMID: 15145991

24. Folland GB, Sitaram A. The uncertainty principle: a mathematical survey. Journal of Fourier analysis and applications. 1997; 3(3):207–238. https://doi.org/10.1007/BF02649110

25. Gabor D. Theory of communication. Part 1: The analysis of information. Journal of the Institution of Electrical Engineers-Part III: Radio and Communication Engineering. 1946; 93(26):429–441.

26. Hsieh IH, Saberi K. Imperfect pitch: Gabor's uncertainty principle and the pitch of extremely brief sounds. Psychonomic bulletin & review. 2016; 23(1):163–171. https://doi.org/10.3758/s13423-015-0863-y PMID: 26022837

27. Qureshi MU, Colebank MJ, Schreier DA, Tabima DM, Haider MA, Chesler NC, et al. Characteristic impedance: frequency or time domain approach? Physiological measurement. 2018; 39(1):014004. https://doi.org/10.1088/1361-6579/aa9d60 PMID: 29176040

28. Anliker M, Histand MB, Ogden E. Dispersion and attenuation of small artificial pressure waves in the canine aorta. Circ Res. 1968; 23(4):539–551. https://doi.org/10.1161/01.RES.23.4.539 PMID: 5677945

29. Abdul-Rahman A, Morgan W, Yu DY. Measurement of normal retinal vascular pulse wave attenuation using modified photoplethysmography. PloS one. 2020; 15(5):e0232523. https://doi.org/10.1371/journal.pone.0232523 PMID: 32379837

30. Allen J. Photoplethysmography and its application in clinical physiological measurement. Physiol Meas. 2007; 28(3):1–59. https://doi.org/10.1088/0967-3334/28/3/R01 PMID: 17322588

31. Betz-Stablein B, Hazelton ML, Morgan WH. Modelling retinal pulsatile blood flow from video data. Stat Methods Med Res. 2016; p. 1575–1584. PMID: 27587593

32. Krovetz LJ, Goldbloom SD. Frequency content of intravascular and intracardiac pressures and their time derivatives. IEEE Transactions on Biomedical Engineering. 1974;(6):498–501. https://doi.org/10.1109/TBME.1974.324344

33. Wiener F, Morkin E, Skalak R, Fishman AP. Wave propagation in the pulmonary circulation. Circ Res. 1966; 19(4):834–850. https://doi.org/10.1161/01.RES.19.4.834 PMID: 5917852

34. Li J. Physical concepts and basic fluid mechanics. In: Dynamics of the vascular system. vol. 1. Singapore: World Scientific Publishing Co Pte Ltd; 2004. p. 41–75.

35. Milnor WR. Hemodynamics. Cardiac dynamics. 1989;.

36. Li JK. Arterial Pulse Transmission Characteristics. In: The Arterial Circulation: Physical Principles and Clinical Applications. Springer Science & Business Media; 2000. p. 69–128.

37. Chen J, Wall M. Epidemiology and risk factors for idiopathic intracranial hypertension. International ophthalmology clinics. 2014; 54(1). https://doi.org/10.1097/IIO.0b013e3182aabf11

38. Fleischman D, Berdahl JP, Zaydlarova J, Stinnett S, Fautsch MP, Allingham RR. Cerebrospinal fluid pressure decreases with older age. PLoS One. 2012; 7(12). https://doi.org/10.1371/journal.pone.0052664 PMID: 23300737

39. Nagaoka T, Yoshida A. The effect of ocular warming on ocular circulation in healthy humans. Archives of Ophthalmology. 2004; 122(10):1477–1481. https://doi.org/10.1001/archopht.122.10.1477 PMID: 15477459

40. Shamshad M, Amitava A, Ahmad I, Wahab S. Changes in central retinal artery blood flow after ocular warming and cooling in healthy subjects. Indian journal of ophthalmology. 2010; 58(3):189. https://doi.org/10.4103/0301-4738.62641 PMID: 20413919

41. Morgan WH, Cringle SJ, Kang MH, Pandav S, Balaratnasingam C, Ezekial D, et al. Optimizing the calibration and interpretation of dynamic ocular force measurements. Graefes Arch Clin Exp Ophthalmol. 2010; 248(3):401–407. https://doi.org/10.1007/s00417-009-1288-y PMID: 20107829

42. R Core Team. R: A Language and Environment for Statistical Computing; 2020. Available from: https://www.R-project.org/.

43. Morgan WH, Abdul-Rahman A, Yu DY, Hazelton ML, Betz-Stablein B, Lind CR. Objective detection of retinal vessel pulsation. PLoS One. 2015; 10(2):e0116475. https://doi.org/10.1371/journal.pone.0116475 PMID: 25643350

44. Artis MJ, Clavel JG, Hoffmann M, Nachane D. Harmonic regression models: A comparative review with applications. Working paper series/Institute for Empirical Research in Economics. 2007;(333).

45. Peterson RA, Cavanaugh JE. Ordered quantile normalization: a semiparametric transformation built for the cross-validation era. Journal of Applied Statistics. 2019; p. 1–16.

46. Yeo IK, Johnson RA. A new family of power transformations to improve normality or symmetry. Biometrika. 2000; 87(4):954–959. https://doi.org/10.1093/biomet/87.4.954

47. Changyong F, Hongyue W, Naiji L, Tian C, Hua H, Ying L, et al. Log-transformation and its implications for data analysis. Shanghai archives of psychiatry. 2014; 26(2):105.

48. Nakagawa S, Schielzeth H. A general and simple method for obtaining R^2 from generalized linear mixed-effects models. Methods Ecol Evol. 2013; 4(2):133–142. https://doi.org/10.1111/j.2041-210x.2012.00261.x

49. Widaman KF, Helm JL, Castro-Schilo L, Pluess M, Stallings MC, Belsky J. Distinguishing ordinal and disordinal interactions. Psychological methods. 2012; 17(4):615. https://doi.org/10.1037/a0030003 PMID: 22984788

50. Morgan WH, Hazelton ML, Yu DY. Retinal venous pulsation: Expanding our understanding and use of this enigmatic phenomenon. Prog Retin Eye Res. 2016; 55:82–107. https://doi.org/10.1016/j.preteyeres.2016.06.003 PMID: 27417037

51. Jacks A, Miller N. Spontaneous retinal venous pulsation: aetiology and significance. J Neurol Neurosurg Psychiatry. 2003; 74(1):7–9. https://doi.org/10.1136/jnnp.74.1.7 PMID: 12486256

52. Levine DN. Spontaneous pulsation of the retinal veins. Microvasc Res. 1998; 56(3):154–165. https://doi.org/10.1006/mvre.1998.2098 PMID: 9828153

53. Golzan SM, Avolio A, Graham SL. Hemodynamic interactions in the eye: a review. Ophthalmologica. 2012; 228(4):214–221. https://doi.org/10.1159/000342157 PMID: 23006897

54. Andersen MS, Pedersen CB, Poulsen FR. A new novel method for assessing intracranial pressure using non-invasive fundus images: a pilot study. Scientific RepoRtS. 2020; 10(1):1–7. https://doi.org/10.1038/s41598-020-70084-0 PMID: 32747697

55. Mittra RA, Sergott RC, Flaharty PM, Lieb WE, Savino PJ, Bosley TM, et al. Optic nerve decompression improves hemodynamic parameters in papilledema. Ophthalmology. 1993; 100(7):987–997. https://doi.org/10.1016/S0161-6420(93)31526-5 PMID: 8321541

56. Querfurth H, Lagrèze WD, Hedges T, Heggerick P. Flow velocity and pulsatility of the ocular circulation in chronic intracranial hypertension. Acta neurologica scandinavica. 2002; 105(6):431–440. https://doi.org/10.1034/j.1600-0404.2002.01273.x PMID: 12027831

57. Kazarians H, Rieper J, Arning C. Hemodynamic alteration of the central retinal artery in idiopathic intracranial hypertension. Aktuelle Neurologie. 2014; 41(01):46–48. https://doi.org/10.1055/s-0034-1367015

58. Morgan WH, Hazelton ML, Azar SL, House PH, Yu DY, Cringle SJ, et al. Retinal venous pulsation in glaucoma and glaucoma suspects. Ophthalmology. 2004; 111(8):1489–1494. https://doi.org/10.1016/j.ophtha.2003.12.053 PMID: 15288976

59. Moret F, Poloschek CM, Lagreze WA, Bach M. Visualization of fundus vessel pulsation using principal component analysis. Invest Ophthalmol Visual Sci. 2011; 52(8):5457–5464. https://doi.org/10.1167/iovs.10-6806 PMID: 21467181

60. Berrett GB, Hogg J, Innes W. Retinal arterial pulsation as an indicator of raised intraocular pressure. SAGE Open Medical Case Reports. 2021; 9:2050313X211054633. https://doi.org/10.1177/2050313X211054633 PMID: 34721875

61. Gangitano J, Sousa FJ. Transient unilateral central retinal artery pulsations secondary to glaucomato-cyclitic crisis and aortic insufficiency. Annals of Ophthalmology. 1980; 12(6):643–644.

62. Arej N, Vasseur V, Jabbour E, Manassero A, Giraud C, Bruneau S, et al. Assessment of Spontaneous Retinal Arterial Pulsations in Acute Central Retinal Vein Occlusions. Journal of ophthalmology. 2020; 2020. https://doi.org/10.1155/2020/3107472 PMID: 33101730

63. Otto T. Modellierung des retinalen Blutflusses durch Auswertung bewegungskorrigierter Angiographie-Bildfolgen; 2000.

64. Schneider U, Wagner AL, Kreissig I. Indocyanine green videoangiography of hemorrhagic retinal arterial macroaneurysms. Ophthalmologica. 1997; 211(2):115–118. https://doi.org/10.1159/000310775 PMID: 9097320

65. Cahuzac A, Scemama C, Mauget-Faÿsse M, Sahel JA, Wolff B. Retinal arterial macroaneurysms: clinical, angiographic, and tomographic description and therapeutic management of a series of 14 cases. European Journal of Ophthalmology. 2016; 26(1):36–43. https://doi.org/10.5301/ejo.5000641 PMID: 26165327

66. Spahr H, Hillmann D, Hain C, Pfäffle C, Sudkamp H, Franke G, et al. Imaging pulse wave propagation in human retinal vessels using full-field swept-source optical coherence tomography. Opt Lett. 2015; 40(20):4771–4774. https://doi.org/10.1364/OL.40.004771 PMID: 26469616

67. Bedggood P, Metha A. Direct measurement of pulse wave propagation in capillaries of the human retina. Optics Letters. 2021; 46(18):4450–4453. https://doi.org/10.1364/OL.434454 PMID: 34525019

68. Garhofer G, Bek T, Boehm AG, Gherghel D, Grunwald J, Jeppesen P, et al. Use of the retinal vessel analyzer in ocular blood flow research. Acta Ophthalmol (Copenh). 2010; 88(7):717–722. https://doi.org/10.1111/j.1755-3768.2009.01587.x PMID: 19681764

69. McHugh JA, D'Antona L, Toma AK, Bremner FD. Spontaneous venous pulsations detected with infrared videography. Journal of Neuro-Ophthalmology. 2020; 40(2):174–177. https://doi.org/10.1097/WNO.0000000000000815 PMID: 31464805

70. Nichols WW, Edwards DG. Arterial elastance and wave reflection augmentation of systolic blood pressure: deleterious effects and implications for therapy. J Cardiovasc Pharmacol Ther. 2001; 6(1):5–21. https://doi.org/10.1177/107424840100600102 PMID: 11452332

71. Moreno AH, Katz AI, Gold LD, Reddy R. Mechanics of distension of dog veins and other very thin-walled tubular structures. Circ Res. 1970; 27(6):1069–1080. https://doi.org/10.1161/01.RES.27.6.1069 PMID: 5494860

72. Keener J, Sneyd J. The circulatory system. In: Mathematical Physiology II: Systems Physiology. New York: Springer-Verlag; 2009. p. 471–522.

73. Feher JJ. Vascular function: Hemodynamics. In: Feher JJ, editor. Quantitative Human Physiology: An introduction. Cambridge, MA, United States: Elsevier-Academic Press; 2012. p. 498–507.

74. Burton AC. Arrangements of Many Vessels. In: Physiology and biophysics of the circulation: an introductory text. 2nd ed. Chicago, United States: Year Book Medical Publishers; 1972. p. 51–62.

75. Caro C, Pedley T, Schroter R. The systemic veins. In: The mechanics of the circulation. Cambridge, United States: Cambridge University Press; 2012. p. 426–466.

76. Hogan MJ, Feeney L. The ultrastructure of the retinal blood vessels: I. The large vessels. J Ultrastruct Res. 1963; 9(1-2):10–28. https://doi.org/10.1016/S0022-5320(63)80035-0 PMID: 14065353

77. Conrad WA. Pressure-flow relationships in collapsible tubes. IEEE Trans Biomed Eng. 1969; 16(4):284–295. https://doi.org/10.1109/TBME.1969.4502660

78. Moses R. Hydrodynamic model eye. Ophthalmologica. 1963; 146(3):137–142. https://doi.org/10.1159/000304511 PMID: 14061447

79. Barami K, Sood S. The cerebral venous system and the postural regulation of intracranial pressure: implications in the management of patients with cerebrospinal fluid diversion. Child's Nervous System. 2016; 32(4):599–607. https://doi.org/10.1007/s00381-015-3010-1 PMID: 26767844

80. Zamir M, Ritman E. Pulsatile flow in an elastic tube. In: The physics of pulsatile flow. Springer, New York, NY; 2000. p. 113–145.

81. Kiel JW. Ocular perfusion pressure, IOP and the ocular Starling resistor effect. In: The ocular circulation. https://www.ncbi.nlm.nih.gov/books/NBK53322/; 2010.

82. Eustace P, Dwyer-Joyce P, Browne M, O'Donohue H. Slit lamp ophthalmodynamometry. Documenta Ophthalmologica. 1977; 44(1):215–217. https://doi.org/10.1007/BF00171475 PMID: 923414

83. Jonas JB. Ophthalmodynamometric measurement of orbital tissue pressure in thyroid-associated orbitopathy. Acta Ophthalmologica Scandinavica. 2004; 82(2):239–239. https://doi.org/10.1111/j.1600-0420.2004.00150a.x PMID: 15043551

84. Morgan WH, Yu DY, Cooper RL, Alder VA, Cringle SJ, Constable IJ. Retinal artery and vein pressures in the dog and their relationship to aortic, intraocular, and cerebrospinal fluid pressures. Microvascular research. 1997; 53(3):211–221. https://doi.org/10.1006/mvre.1997.2010 PMID: 9211399

85. Luckie AP, Wroblewski JJ, Bird AC, Hamilton AP, Sanders MD, Green W, et al. The venous closing pressure in central retinal vein obstruction. Aust N Z J Ophthalmol. 1996; 24(3):233–238. https://doi.org/10.1111/j.1442-9071.1996.tb01585.x PMID: 8913125

86. Armentano RL, Fischer EIC, Cymberknop LJ. Damping in the vascular wall;.

87. Vlachopoulos C, O'Rourke M, Nichols WW. Properties of the arterial wall: practice. In: McDonald's blood flow in arteries: theoretical, experimental and clinical principles. CRC press; 2011.

88. Salvi P. Central Blood Pressure: Part 1. Pathophysiology. In: Pulse Waves. How Vascular Hemodynamics Affects Blood Pressure. Springer; 2017. p. 83–111.

89. Evans DW, Hosking SL, Embleton SJ, Morgan AJ, Bartlett JD. Spectral content of the intraocular pressure pulse wave: glaucoma patients versus normal subjects. Graefe's archive for clinical and experimental ophthalmology. 2002; 240(6):475–480. https://doi.org/10.1007/s00417-002-0460-4 PMID: 12107515

90. Božić M, Dukić ML, Stojković M. Spectral analysis of intraocular pressure pulse wave in open angle glaucomas and healthy eyes. Current Eye Research. 2012; 37(11):1019–1024. https://doi.org/10.3109/02713683.2012.700755 PMID: 22730930

91. Choi J, Lee J, Park SB, Lee KS, Sung KR, Kook MS. Factors affecting ocular pulse amplitude in eyes with open angle glaucoma and glaucoma-suspect eyes. Acta ophthalmologica. 2012; 90(6):552–558. https://doi.org/10.1111/j.1755-3768.2010.01954.x PMID: 20560890

92. Takizawa H, Sugiura K, Baba M, Tachizawa T, Kamatsuka E, Hayama N. Spectral analysis of cerebrospinal fluid pulse wave. No to Shinkei Brain and Nerve. 1983; 35(12):1223–1227. PMID: 6671074

93. Jonas JB, Wang N, Yang D, Ritch R, Panda-Jonas S. Facts and myths of cerebrospinal fluid pressure for the physiology of the eye. Prog Retin Eye Res. 2015; 46:67–83. https://doi.org/10.1016/j.preteyeres.2015.01.002 PMID: 25619727

94. London A, Benhar I, Schwartz M. The retina as a window to the brain—from eye research to CNS disorders. Nature Reviews Neurology. 2013; 9(1):44–53. https://doi.org/10.1038/nrneurol.2012.227 PMID: 23165340

95. van de Kreeke JA, Nguyen HT, Konijnenberg E, Tomassen J, den Braber A, Ten Kate M, et al. Retinal and cerebral microvasculopathy: relationships and their genetic contributions. Investigative ophthalmology & visual science. 2018; 59(12):5025–5031. https://doi.org/10.1167/iovs.18-25341

96. Trost A, Lange S, Schroedl F, Bruckner D, Motloch KA, Bogner B, et al. Brain and retinal pericytes: origin, function and role. Frontiers in cellular neuroscience. 2016; 10:20. https://doi.org/10.3389/fncel.2016.00020 PMID: 26869887

97. Zong Y, Xu H, Yu J, Jiang C, Kong X, He Y, et al. Retinal vascular autoregulation during phase IV of the valsalva maneuver: an optical coherence tomography angiography study in healthy Chinese adults. Frontiers in Physiology. 2017; 8:553. https://doi.org/10.3389/fphys.2017.00553 PMID: 28804464

98. Fischer WS, Wall M, McDermott MP, Kupersmith MJ, Feldon SE. Photographic reading center of the Idiopathic Intracranial Hypertension Treatment Trial (IIHTT): methods and baseline results. Investigative ophthalmology & visual science. 2015; 56(5):3292–3303. https://doi.org/10.1167/iovs.15-16465 PMID: 26024112